Journal of
Ceramic Science
and Technology

J. Ceram. Sci. Technol., **09** [2] 163-174 (2018)
DOI: 10.4416/JCST2017-00095
available online at: http://www.ceramic-science.com

Effect of Multiple loading sequence on in-phase thermomechanical fatigue hysteresis of silicon carbide fiber-reinforced ceramic-matrix composites

L. Li*

College of Civil Aviation, Nanjing University of Aeronautics and Astronautics, No.29 Yudao St., Nanjing 210016, PR China

received November 27, 2017; received in revised form December 28, 2017; accepted January 29, 2018

Abstract

In this paper, the effect of multiple loading sequence on the in-phase (IP) thermomechanical fatigue (TMF) hysteresis of silicon carbide fiber-reinforced ceramic-matrix composites (SiC-CMCs) has been investigated. Considering the coupling effects of multiple loading sequence, thermal cyclic temperature and applied cycle number, the fiber/matrix interface damage lengths have been determined based on the thermomechanical micromechanical stress field and fracture mechanics method. The relationships between the in-phase TMF hysteresis loops, multiple loading sequence, thermal cyclic temperature and fiber/matrix interface damage state have been established. The in-phase TMF stress/strain hysteresis loops and fiber/matrix interface damage state for different composite material properties, peak stress with different loading sequence and damage state have been discussed. The comparisons of the in-phase TMF stress/strain hysteresis loops and fiber/matrix interface damage between single peak stress and multiple loading sequence have been analyzed. The TMF stress/strain hysteresis loops and fiber/matrix interface damage state of 2D SiC/SiC composite subjected to low-high three loading sequences have been predicted. Under TMF multiple loading sequence, the fiber/matrix interface slip lengths are larger than those under TMF single peak stress, leading to the increase of TMF stress/strain hysteresis loops area, peak and residual strain, and the decrease of hysteresis modulus.

Keywords: Ceramic-matrix composites (CMCs), thermomechanical fatigue, hysteresis loops, multiple loading sequence

I. Introduction

Silicon carbide fiber-reinforced ceramic matrix composites (SiC-CMCs) possess high specific strength and high specific modulus at elevated temperature, and are a breakthrough materials technology for jet engines[1,2]. SiC-CMCs components are being designed and tested in commercial and military aeroengines[3]. CFM's newest engine introduces the use of a large SiC-CMC turbine shroud. The GE9X, GE's replacement for its GE90 engine powering Boeing's 777, will incorporate five different types of SiC-CMC parts[4].

Under TMF loading, the thermal cyclic temperature changes with decreasing or increasing applied stress upon unloading or reloading[5]. The coupling of the temperature and stress field leads to much more serious damage evolution in fiber-reinforced CMCs subjected to TMF loading than that under cyclic loading at constant elevated temperature[6,7]. Under tension-tension or tension-compression cyclic loading at constant elevated temperature, the cyclic loading behavior of C/SiC, SiC/SiC and oxide/oxide composites in different testing environments (i.e. air or combustion environment) has been analyzed[8,9,10,11,12]. The damage evolution of modulus, strain and residual strength depended on the stress level, testing temperature and environments. Li[13] investigated the out-of-phase (OP) TMF hysteresis loops of fiber-reinforced CMCs subjected to single-peak stress. The coupling effects of thermal cyclic temperature and fiber/matrix interface damage upon cyclic loading/unloading have been considered. However, under multiple-loading sequences, the TMF hysteresis loops and fiber/matrix interface damage depend on the peak stress level and loading sequence. In the research mentioned above, the effect of a multiple-loading sequence on the TMF hysteresis loops of fiber-reinforced CMCs has not been investigated.

The objective of this paper is to investigate the effect of a multiple-loading sequence on the in-phase TMF stress/strain hysteresis loops of SiC-fiber-reinforced CMCs. With consideration of the thermal and mechanical coupling, the TMF microstress field upon loading/unloading in-phase TMF cycling is analyzed. The in-phase TMF stress/strain hysteresis loops and fiber/matrix interface damage conditions for different composite material properties, peak stress with different loading sequence and damage state are discussed. Comparisons of the in-phase TMF stress/strain hysteresis loops and fiber/matrix interface damage between single-peak stress and a multiple loading sequence are analyzed. The TMF stress/strain hysteresis loops and fiber/matrix interface damage state

* Corresponding author: llb451@nuaa.edu.cn

of the 2D SiC/SiC composite subjected to three low-high loading sequences are predicted.

II. Theoretical Analysis

Under TMF loading, the thermal cyclic temperature changes with decreasing or increasing applied stress upon unloading or reloading. The variation of the thermal cyclic temperature and peak stress with increasing applied cycles can be divided into three different cases, as shown in Fig. 1, including:

(1) Case 1, single-peak stress under in-phase TMF loading;
(2) Case 2, low-high peak stress under in-phase TMF loading;
(3) Case 3, high-low peak stress under in-phase TMF loading.

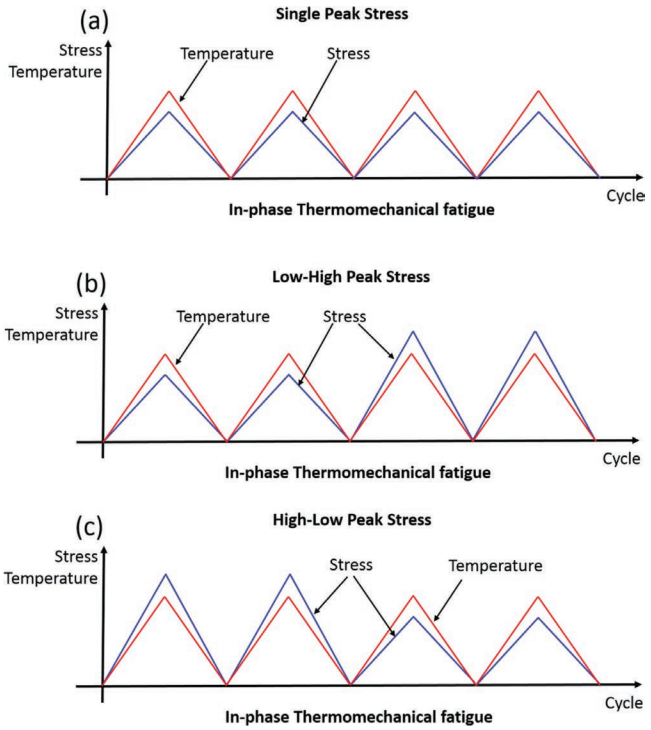

Fig. 1: The schematic of in-phase thermomechanical fatigue loading subjected to (a) single-peak stress; (b) low-high peak stress; and (c) high-low peak stress.

(1) TMF interface damage models

The coupling of thermal cyclic temperature and stress field affects the fiber/matrix interface damage state especially subjected to a multiple-loading sequence, i.e. Case 2 and Case 3 in Fig. 1. Upon first loading to the fatigue peak stress of σ_{max1}, it is assumed that matrix multicracking and fiber/matrix interface debonding occur. To analyze stress distributions in the fiber and the matrix, a unit cell is extracted from the ceramic matrix composites, as shown in Fig. 2. The unit cell contains a single fiber surrounded by a hollow cylinder of matrix. The fiber radius is r_f, and the matrix radius is $R(R = r_f/V_f^{1/2})$. The length of the unit cell is $l_c/2$, which is half of the matrix crack space. The fiber/matrix interface debonding length is l_d. On the matrix crack plane, the fibers carry all the applied stress (i.e. σ/V_f, where σ denotes far-field applied stress and V_f denotes fiber volume fraction). After experiencing N_1 applied cycles, the fiber/matrix interface shear stress in the interface debonded region degrades due to the interface wear and/or interface oxidation[14, 15, 16, 17, 18, 19, 20, 21, 22, 23, 24, 25, 26, 27, 28]. The cyclic and temperature-dependent fiber/matrix interface shear stress can be described using the following equation[29].

$$\tau_i(T, N) = \tau_0(N) + \mu \frac{|\alpha_{rf} - \alpha_{rm}|(T_0 - T)}{A} \quad (1)$$

where μ denotes the fiber/matrix interface frictional coefficient[30, 31]; α_{rf} and α_{rm} denote the radial thermal expansion coefficient of the fiber and the matrix, respectively; A is a constant depending on the elastic properties of the matrix and fibers[29]; and $\tau_0(N)$ denotes the cyclic-dependent interface shear stress[32]. When the fatigue peak stress increases from σ_{max1} to σ_{max2}, the fiber/matrix interface debonded length continues to propagate along the interface. Upon unloading from σ_{max2}, the fiber/matrix interface debonded region can be divided into three regions, i.e. interface counter-slip region with the interface shear stress of $\tau_i(T, N_1)$, interface counter-slip region with the interface shear stress of $\tau_i(T, N–N_1)$ and interface slip region with the interface shear stress of $\tau_i(T, N–N_1)$. Upon reloading to σ_{max2}, the fiber/matrix interface debonded length can be divided into four regions, i.e. interface new-slip region with the interface shear stress of $\tau_i(T, N_1)$, interface counter-slip region with the interface shear stress of $\tau_i(T, N_1)$, interface counter-slip region with the interface shear stress of $\tau_i(T, N–N_1)$ and interface slip region with the interface shear stress of $\tau_i(T, N–N_1)$. The fiber/matrix interface debonded length and interface slip length are determined using the following equation[33]

$$\zeta_d = \frac{F}{4\pi r_f} \frac{\partial w_f(0)}{\partial l_d} - \frac{1}{2}\int_0^{l_d} \tau_i(T, N) \frac{\partial v(x)}{\partial l_d} dx \quad (2)$$

where ζ_d denotes the fiber/matrix interface debonded energy; $F(=\pi r_f^2\sigma/V_f)$ is the fiber load at the matrix cracking plane; $w_f(0)$ denotes the fiber axial displacement at the matrix crack plane; and $v(x)$ denotes the relative displacement between the fiber and the matrix.

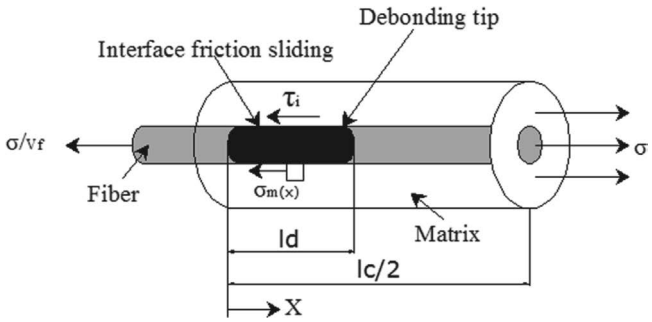

Fig. 2: The unit cell of shear-lag model.

Under thermomechanical fatigue peak stress of σ_{max1} for N_1 applied cycles, the fiber/matrix interface debonded length (l_d), unloading interface counter-slip length (y) and reloading interface new-slip length (z) can be described using the following equations.

$$l_d(\sigma_{max\,1},T,N_1)=\frac{r_f}{2}\left(\frac{V_mE_m\sigma_{max\,1}}{V_fE_c\tau_i(T,N_1)}-\frac{1}{\rho}\right)-\sqrt{\left(\frac{r_f}{2\rho}\right)^2+\frac{r_fV_mE_mE_f}{E_c\tau_i^2(T,N_1)}\zeta_d} \tag{3}$$

$$y(\sigma_{max\,1},T,N_1)=\frac{1}{2}\left\{l_d(\sigma_{max\,1})-\left[\frac{r_f}{2}\left(\frac{V_mE_m\sigma_{min}}{V_fE_c\tau_i(T,N_1)}-\frac{1}{\rho}\right)-\sqrt{\left(\frac{r_f}{2\rho}\right)^2+\frac{r_fV_mE_mE_f}{E_c\tau_i^2(T,N_1)}\zeta_d}\right]\right\} \tag{4}$$

$$z(\sigma_{max\,1},T,N_1)=y(\sigma_{min})-\frac{1}{2}\left\{l_d(\sigma_{max\,1})-\left[\frac{r_f}{2}\left(\frac{V_mE_m\sigma_{max\,1}}{V_fE_c\tau_i(T,N_1)}-\frac{1}{\rho}\right)-\sqrt{\left(\frac{r_f}{2\rho}\right)^2+\frac{r_fV_mE_mE_f}{E_s\tau_i^2(T,N_1)}\zeta_d}\right]\right\} \tag{5}$$

where V_m denotes the matrix volume fraction; ϱ denotes the shear-lag model parameter[34]; E_f denotes the fiber axial elastic modulus; E_m denotes the matrix elastic modulus; and E_c denotes the composite elastic modulus along the longitudinal fiber direction.

Upon increasing thermomechanical fatigue peak stress from σ_{max1} to σ_{max2}, the new fiber/matrix interface debonding and sliding lengths are affected by the stress level and interface wear regions and can be described using the following equations:

$$l_d(\sigma_{max\,2},T,N)=\left(1-\frac{\tau_i(T,N_1)}{\tau_i(T,N-N_1)}\right)l_d(\sigma_{max\,1},T,N)+\frac{r_f}{2}\left(\frac{V_mE_m\sigma_{max\,2}}{V_fE_c\tau_i(T,N-N_i)}-\frac{1}{\rho}\right)-\sqrt{\left(\frac{r_f}{2\rho}\right)^2+\frac{r_fV_mE_mE_f}{E_c\tau_i^2(T,N-N_1)}\zeta_d} \tag{6}$$

$$y(\sigma_{min},T,N)=\frac{1}{2}\left\{l_d(\sigma max\,2)+\left(1-\frac{\tau_i(T,N_1)}{\tau_i(T,N-N_1)}\right)l_d(\sigma_{max\,1})-\left[\frac{r_f}{2}\left(\frac{V_mE_m}{V_fE_c}\frac{\sigma_{min}}{\tau_i(T,N-N_i)}-\frac{1}{\rho}\right)-\sqrt{\left(\frac{r_f}{2\rho}\right)^2+\frac{r_fV_mE_mE_f}{E_c\tau_i^2(T,N-N_1)}\zeta_d}\right]\right\} \tag{7}$$

$$z(\sigma_{max\,2},T,N)=\frac{\tau_i(T,N-N_1)}{\tau_i(T,N_1)}\left\{y(\sigma_{min})-\frac{1}{2}\left[l_d(\sigma_{max\,2})+\left(1-\frac{\tau_i(T,N_1)}{\tau_i(T,N-N_1)}\right)l_d(\sigma_{max\,1})-\left[\frac{r_f}{2}\left(\frac{V_mE_m}{V_fE_c}\frac{\sigma}{\tau_i(T,N-N_1)}-\frac{1}{\rho}\right)-\sqrt{\left(\frac{r_f}{2\rho}\right)^2+\frac{r_fV_mE_mE_f}{E_c\tau_i^2(T,N-N_1)}\zeta_d}\right]\right]\right\} \tag{8}$$

(2) TMF hysteresis models

Under TMF loading at the peak stress of σ_{max1}, the unloading and reloading composite strain can be determined using the following equations:

$$\varepsilon_{unloading}=\frac{\sigma}{V_fE_f}+4\frac{\tau_i(T,N_1)}{E_f}\frac{y^2}{r_fl_c}-2\frac{\tau_i(T,N_1)}{E_f}\frac{(2y-l_d)(2y+l_d-l_c)}{r_fl_c}-(\alpha_{lc}-\alpha_{lf})\Delta T \tag{9}$$

$$\varepsilon_{reloading}=\frac{\sigma}{V_fE_f}-4\frac{\tau_i(T,N_1)}{E_f}\frac{z^2}{r_fl_c}+4\frac{\tau_i(T,N_1)}{E_f}\frac{(y-2z)^2}{r_fl_c}+2\frac{\tau_i(T,N_1)}{E_f}\frac{(l_d-2y+2z)(l_d+2y-2z-l_c)}{r_fl_c}-(\alpha_{lc}-\alpha_{lf})\Delta T \tag{10}$$

where α_{lc} and α_{lf} denote the composite and fiber axial thermal expansion coefficient, respectively; and ΔT denotes the temperature difference between the fabricated temperature and testing temperature.

Under TMF loading at the second peak stress of σ_{max2}, the unloading and reloading composite strain can be determined using the following equations:

$$\varepsilon_{unloading}=\frac{2\sigma l_d}{V_fE_fl_c}+\frac{2\tau_i(T,N_1)}{r_fE_fl_c}\xi^2+\frac{4\tau_i(T,N_1)}{r_fE_fl_c}\xi(l_d-\xi)+\frac{4\tau_i(T,N-N_1)}{r_fE_fl_c}(y-\xi)^2-\frac{2\tau_i(T,N-N_1)}{r_fE_fl_c}(2y-\xi-l_d)^2+\frac{2\sigma_{fo}}{E_fl_c}\left(\frac{l_c}{2}-l_d\right)+\frac{2r_f}{\rho E_fl_c}\left[\frac{V_m}{V_f}\sigma_{mo}+\frac{2\tau_i(T,N_1)}{r_f}\xi+\frac{2\tau_i(T,N-N_1)}{r_f}(2y-\xi-l_d)\right]\times\left[1-\exp\left(-\rho\frac{l_c/2-l_d}{r_f}\right)\right]-(\alpha_{lc}-\alpha_{lf})\Delta T \tag{11}$$

$$\varepsilon_{reloading} = \frac{2\sigma}{V_f E_f l_c} l_d - \frac{4\tau_i(T, N_1)}{r_f E_f l_c} z^2 + \frac{2\tau_i(T, N_1)}{r_f E_f l_c}(2z - \xi)^2 - \frac{4\tau_i(T, N_1)}{r_f E_f l_c}(2z - \xi)(l_d - \xi) + \frac{4\tau_i(T, N - N_1)}{r_f E_f l_c}(y - \xi)^2 - \frac{2\tau_i(T, N - N_1)}{r_f E_f l_c}(2y - \xi - l_d)^2 + \frac{2\sigma_{fo}}{E_f l_c}\left(\frac{l_c}{2} - l_d\right) + \frac{2r_f}{\rho E_f l_c}\left[\frac{V_m}{V_f}\sigma_{mo} - \frac{2\tau_i(T, N_i)}{r_f}(2z - \xi) + \frac{2\tau_i(T, N - N_i)}{r_f}(2y - \xi - l_d)\right] \times \left[1 - \exp\left(-\rho\frac{l_c/2 - l_d}{r_f}\right)\right] - (\alpha_{lc} - \alpha_{lf})\Delta T \quad (12)$$

III. Results and Discussions

The in-phase TMF stress/strain hysteresis loops and fiber/matrix interface damage state for different composite material properties, peak stress with different loading sequence and damage state are discussed. The comparisons of in-phase TMF stress/strain hysteresis loops and fiber/matrix interface damage between single-peak stress and multiple-loading sequence are analyzed. The SiC/SiC composite is used for the case study and its material properties are given by[29]: V_f =30 %, E_f =230 GPa, E_m =300 GPa, r_f =7.5 μm, ζ_d =0.1 J/m^2, α_{rf} =2.9×10^{-6}/K, α_{lf} =3.9×10^{-6}/K, α_{rm} =4.6×10^{-6}/K, α_{lm} =2.0 × 10^{-6}/K.

(1) Effect of material properties

The effect of fiber volume content (i.e. V_f =30 % and 35 %), fiber/matrix interface frictional shear stress (i.e. τ_0 =10 and 20 MPa), fiber/matrix interface fracture energy (i.e. ζ_d = 0.1 and 0.2 J/m^2) and fiber/matrix interface frictional coefficient (i.e. μ = 0.1 and 0.2) on the in-phase TMF stress/strain hysteresis loops and fiber/matrix interface damage state subjected to a multiple-loading sequence of σ_{max1} =120 MPa and σ_{max2} =180 MPa at the thermal cyclic temperature range of T_1 = 100 °C and T_2 = 800 °C are shown in Figs. 3 ~ 5.

When V_f = 30 % and 35 %, the TMF stress/strain hysteresis loops correspond to the partial debonding and sliding in the fiber/matrix interface debonded region; the fiber/matrix interface new-slip and counter-slip lengths can be divided into two regions, due to the low fiber/matrix interface shear stress in the interface wear region. With increasing fiber volume content from 30 % to 35 %, the fiber/matrix interface slip range decreases from 67 % to 52 %; the TMF stress/strain hysteresis loops' area decreases from 37.3 kJ/m^3 to 22.9 kJ/m^3; the peak strain decreases from 0.19 % to 0.14 %; the residual strain decreases from 0.049 % to 0.03 %; and the hysteresis modulus increases from 127 GPa to 163 GPa, as shown in Fig. 3.

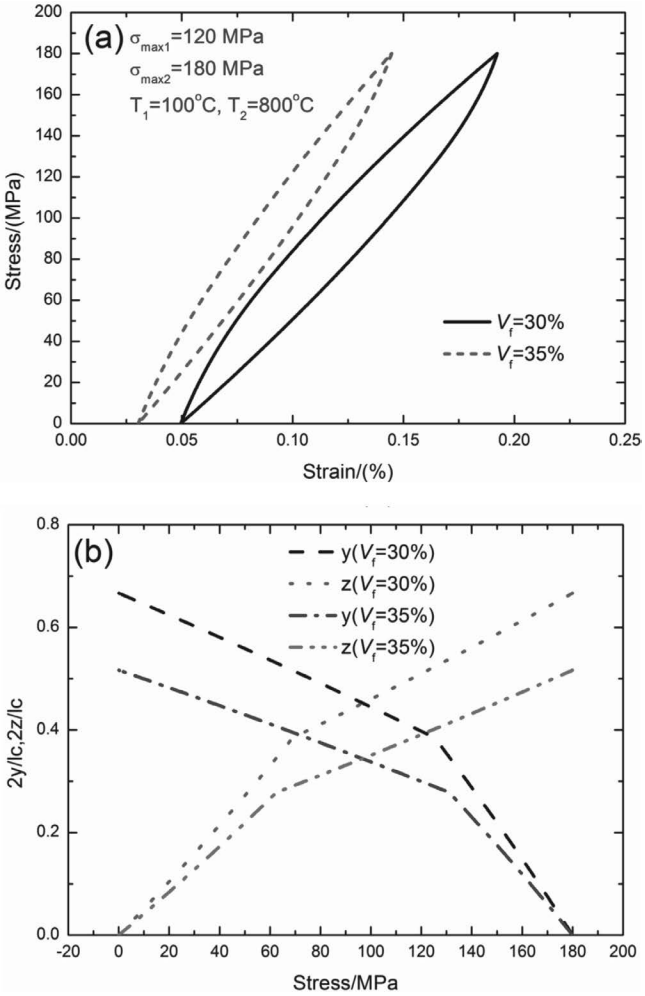

Fig. 3: The effect of fiber volume fraction (V_f =30 % and 35 %) on (a) in-phase thermomechanical fatigue hysteresis loops; and (b) the fiber/matrix interface slip length of a SiC/SiC composite under multiple loading sequence of σ_{max1} =120 MPa and σ_{max2}=180 MPa at the temperature range of T_1=100 °C and T_2=800 °C.

When τ_0 =10 and 20 MPa, the TMF stress/strain hysteresis loops correspond to the partial debonding and sliding in the fiber/matrix interface debonded region; with increasing fiber/matrix interface frictional shear stress from 10 to 20 MPa, the fiber/matrix interface slip range decreases from 69 % to 40 %; the TMF stress/strain hysteresis loops' area decreases from 33.5 kJ/m^3 to 16.8 kJ/m^3; the peak strain decreases from 0.171 % to 0.128 %; the residual strain decreases from 0.046 % to 0.022 %; and the hysteresis modulus increases from 144 GPa to 170 GPa, as shown in Fig. 4.

When ζ_d = 0.1 and 0.2 J/m^2, the TMF stress/strain hysteresis loops correspond to the partial debonding and sliding in the fiber/matrix interface debonded region; with increasing fiber/matrix interface fracture energy from 0.1 to 0.2 J/m^2, the fiber/matrix interface slip range decreases from 47 % to 43 %; the TMF stress/strain hysteresis loops' area decreases from 19.9 kJ/m^3 to 18 kJ/m^3; the peak strain decreases from 0.134 % to 0.125 %; the residual strain decreases from 0.025 % to 0.02 %; and the hysteresis modulus increases from 165 GPa to 171 GPa, as shown in Fig. 5.

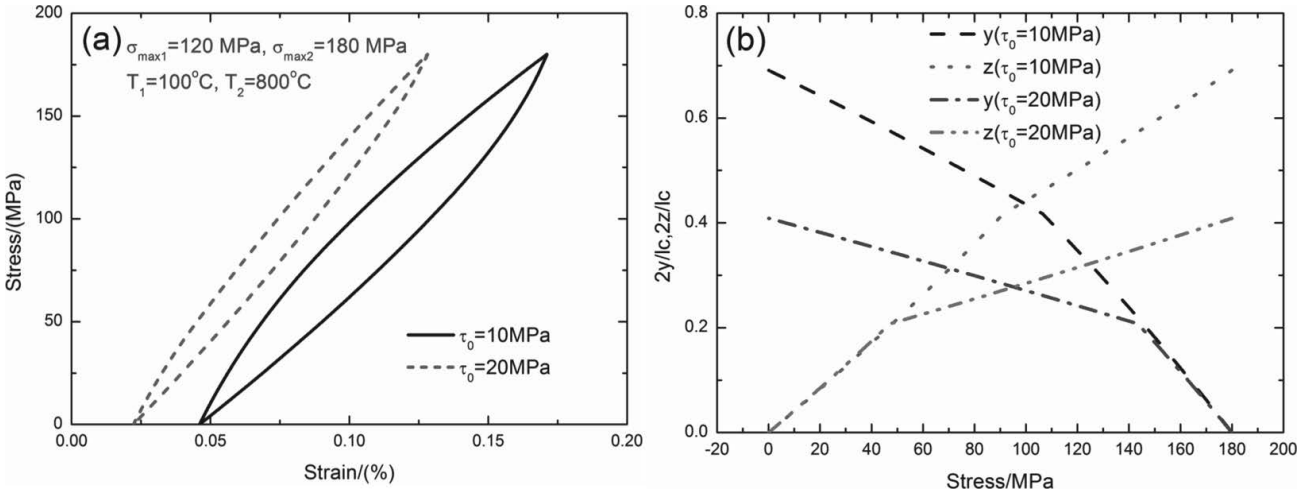

Fig. 4: The effect of fiber/matrix interface shear stress (τ_0 = 10 and 20 MPa) on (a) in-phase thermomechanical fatigue hysteresis loops; and (b) the fiber/matrix interface slip length of SiC/SiC composite under multiple loading sequence of σ_{max1} = 120 MPa and σ_{max2} = 180 MPa at the thermal cyclic temperature range of T_1 = 100 °C and T_2 = 800 °C.

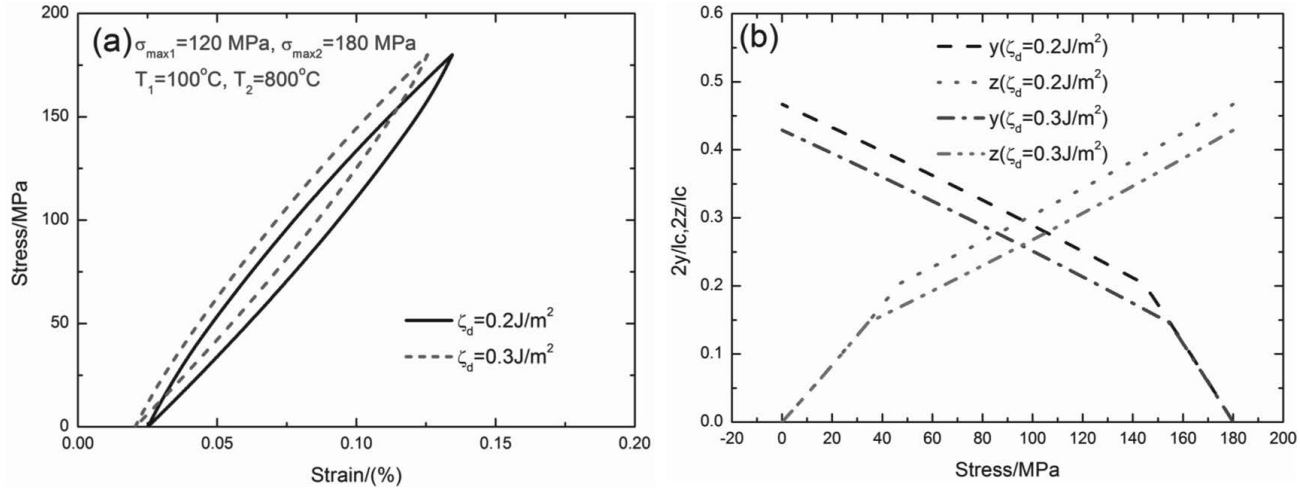

Fig. 5: The effect of fiber/matrix interface debonded energy (ζ_d = 0.2 and 0.3 J/m^2) on (a) in-phase thermomechanical fatigue hysteresis loops; and (b) the fiber/matrix interface slip length of SiC/SiC composite under multiple loading sequence of σ_{max1} = 120 MPa and σ_{max2} = 180 MPa at the thermal cyclic temperature range of T_1 = 100 °C and T_2 = 800 °C.

When μ =0.1 and 0.2, the TMF stress/strain hysteresis loops correspond to the partial debonding and sliding in the fiber/matrix interface debonded region; with increasing fiber/matrix interface frictional coefficient from 0.1 to 0.2, the fiber/matrix interface slip range decreases from 33 % to 24 %; the TMF stress/strain hysteresis loops' area decreases from 18 kJ/m^3 to 14.1 kJ/m^3; the peak strain decreases from 0.123 % to 0.109 %; the residual strain decreases from 0.039 % to 0.038 %; and the hysteresis modulus increases from 214 GPa to 253 GPa, as shown in Fig. 6.

(2) Effect of peak stress with a low-high multiple-loading sequence

The effect of the TMF first peak stress (i.e. σ_{max1} =100 and 140 MPa) and second peak stress (i.e. σ_{max2} =140 and 160 MPa) on the in-phase TMF stress/strain hysteresis loops and fiber/matrix interface damage state subjected to a low-high multiple-loading sequence of σ_{max2} =180 MPa and σ_{max1} =120 MPa at the thermal cyclic temperature range of T_1 = 100 °C and T_2 = 800 °C are shown in Figs. 7 and 8.

When σ_{max1} =100 and 140 MPa, the TMF stress/strain hysteresis loops under σ_{max2} = 180 MPa correspond to the partial debonding and sliding in the fiber/matrix interface debonded region; with increasing TMF first peak stress from 100 to 140 MPa, the fiber/matrix interface slip range increases from 47 % to 56 %; the TMF stress/strain hysteresis loops' area increases from 20.1 kJ/m^3 to 26.1 kJ/m^3; the peak strain increases from 0.137 % to 0.151 %; the residual strain increases from 0.028 % to 0.032 %; and the hysteresis modulus decreases from 165 GPa to 151 GPa, as shown in Fig. 7.

When σ_{max2} =140 and 160 MPa, the TMF stress/strain hysteresis loops correspond to the partial debonding and sliding in the fiber/matrix interface debonded region; with increasing second peak stress from 140 to 160 MPa, the fiber/matrix interface slip range increases from 44 % to 48 %; the TMF stress/strain hysteresis loops' area increases from 12.1 kJ/m^3 to 16.9 kJ/m^3; the peak strain increases from 0.101 % to 0.122 %; the residual strain increases from 0.018 % to 0.023 %; and the hysteresis modulus decreases from 168 GPa to 161 GPa, as shown in Fig. 8.

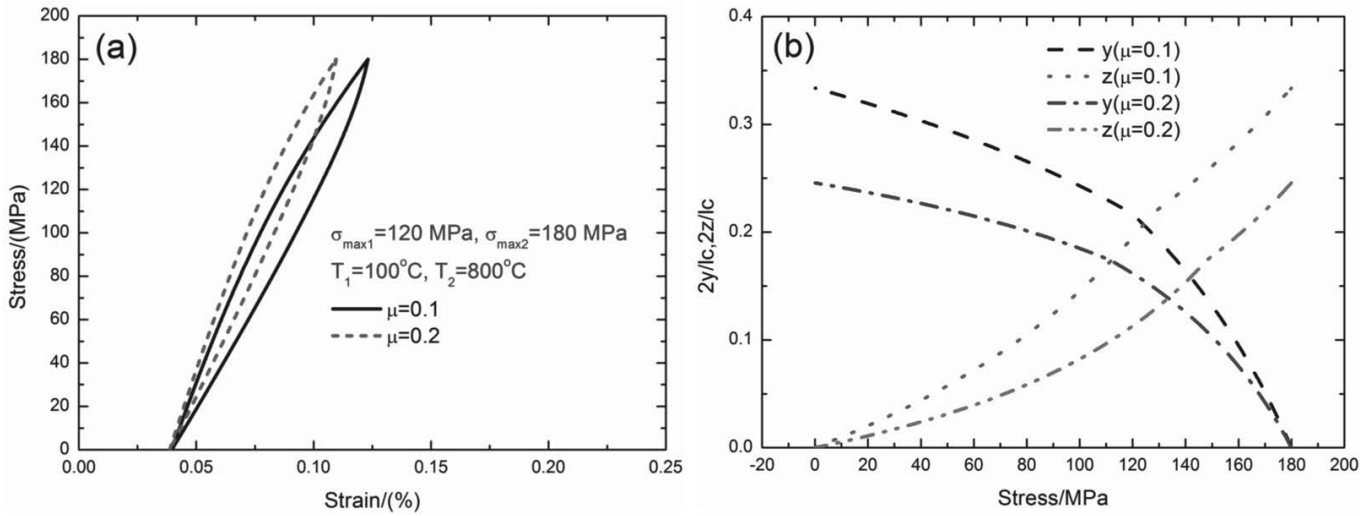

Fig. 6: The effect of fiber/matrix interface frictional coefficient (μ = 0.1 and 0.2) on (a) in-phase thermomechanical fatigue hysteresis loops; and (b) the fiber/matrix interface slip length of SiC/SiC composite under a multiple loading sequence of σ_{max1} = 120 MPa and σ_{max2} = 180 MPa at the thermal cyclic temperature range of T_1 =100 °C and T_2 =800 °C.

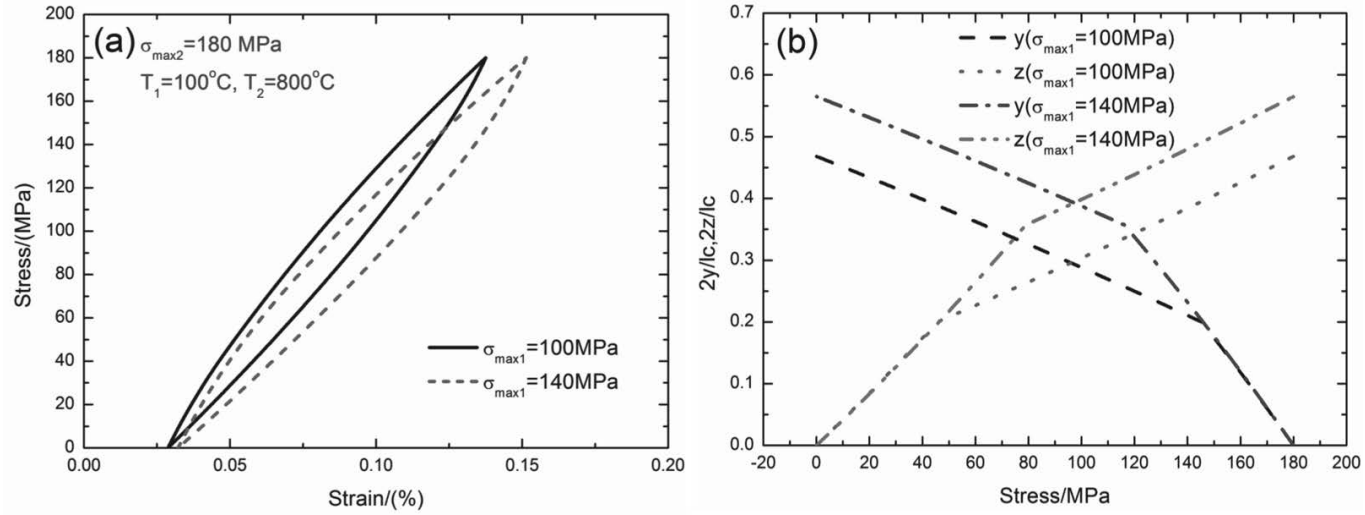

Fig. 7: The effect of the first peak stress (σ_{max1} = 100 MPa and 140 MPa) on (a) in-phase thermomechanical fatigue hysteresis loops; and (b) the fiber/matrix interface slip length of SiC/SiC composite under a low-high multiple loading sequence of σ_{max2} =180 MPa at the thermal cyclic temperature range of T_1 = 100 °C and T_2 = 800 °C.

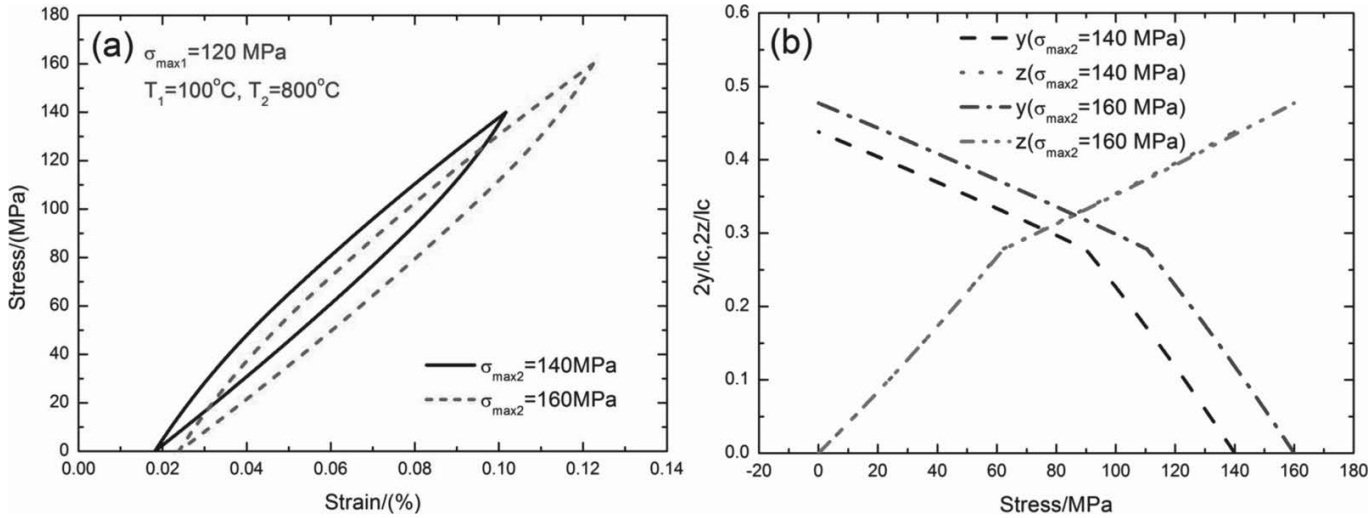

Fig. 8: The effect of second peak stress (σ_{max2} = 140 and 160 MPa) on (a) in-phase thermomechanical fatigue hysteresis loops; and (b) the fiber/matrix interface slip length of SiC/SiC composite under a low-high multiple loading sequence of σ_{max1} =120 MPa at the thermal cyclic temperature range of T_1 =100 °C and T_2 =800 °C.

(3) Effect of peak stress with a high-low multiple-loading sequence

The effect of the TMF first peak stress (i.e. σ_{max1} = 140 and 180 MPa) and second peak stress (i.e. σ_{max2} = 120 and 140 MPa) on the in-phase TMF stress/strain hysteresis loops and fiber/matrix interface damage state subjected to the high-low multiple-loading sequence of σ_{max2} = 120 MPa and σ_{max1} =180 MPa at the thermal cyclic temperature range of T_1 = 100 °C and T_2 = 800 °C is shown in Figs. 9 and 10.

When σ_{max1} = 140 and 180 MPa, the TMF stress/strain hysteresis loops under σ_{max2} =120 MPa correspond to the partial debonding and sliding in the fiber/matrix interface debonded region; with increasing TMF first peak stress from 140 to 180 MPa, the fiber/matrix interface slip range increases from 44.7 % to 54.4 %; the TMF stress/strain hysteresis loops' area increases from 9.8 kJ/m^3 to 12.2 kJ/m^3; the peak strain increases from 0.086 % to 0.093 %; the residual strain increases from 0.015 % to 0.019 %; and the hysteresis modulus decreases from 169 GPa to 162 GPa, as shown in Fig. 9.

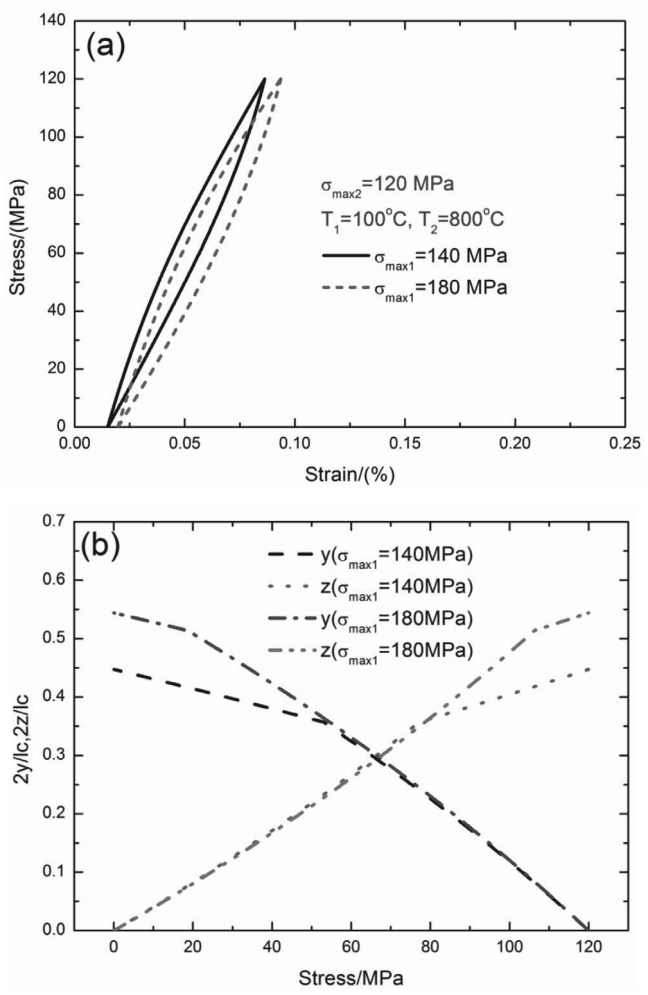

Fig. 9: The effect of the first peak stress (σ_{max1} =140 MPa and 180 MPa) on (a) in-phase thermomechanical fatigue hysteresis loops; and (b) the fiber/matrix interface slip length of SiC/SiC composite under a high-low multiple loading sequence of σ_{max2} =120 MPa at the thermal cyclic temperature range of T_1 = 100 °C and T_2 = 800 °C.

When σ_{max2} =120 and 140 MPa, the TMF stress/strain hysteresis loops correspond to the partial debonding and sliding in the fiber/matrix interface debonded region; with increasing second peak stress from 120 to 140 MPa, the fiber/matrix interface slip range increases from 54 % to 58 %; the TMF stress/strain hysteresis loops' area increases from 12.2 kJ/m^3 to 18.1 kJ/m^3; the peak strain increases from 0.093% to 0.115%; the residual strain increases from 0.0196 % to 0.0247 %; and the hysteresis modulus decreases from 163 GPa to 155 GPa, as shown in Fig. 10.

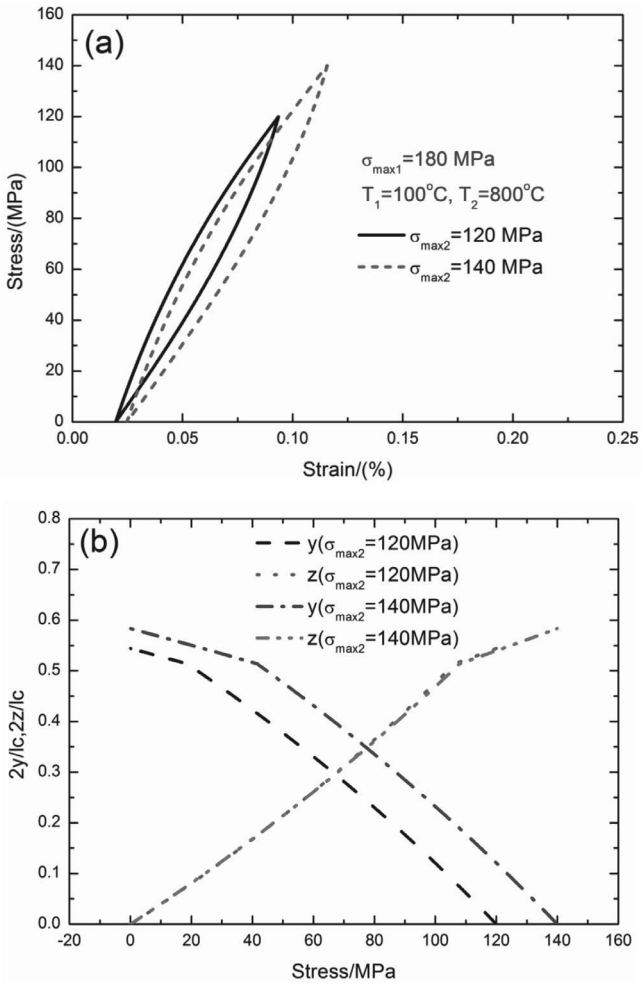

Fig. 10: The effect of the second peak stress (σ_{max2} = 120 and 140 MPa) on (a) in-phase thermomechanical fatigue hysteresis loops; and (b) the fiber/matrix interface slip length of SiC/SiC composite under a high-low multiple loading sequence of σ_{max1} =180 MPa at the thermal cyclic temperature range of T_1 = 100 °C and T_2 = 800 °C.

(4) Effect of damage state

The effect of matrix crack spacing (i.e. l_c =200 and 300 μm), cycle number (i.e. N = 1, 10 and 100) and thermal cyclic temperature range (i.e., T_1 = 100 °C, T_2 = 800 °C and T_1=200 °C, T_2 = 600 °C) on the in-phase TMF stress/strain hysteresis loops and fiber/matrix interface damage state subjected to a multiple-loading sequence of σ_{max1} =120 MPa and σ_{max2} = 180 MPa at the thermal cyclic temperature range of T_1 = 100 °C and T_2 = 800 °C is given in Figs. 11 ~ 13.

When l_c =200 and 300 μm, the TMF stress/strain hysteresis loops correspond to the partial debonding and sliding in the fiber/matrix interface debonded region; with

increasing matrix crack spacing from 200 to 300 μm, the fiber/matrix interface slip range decreases from 64 % to 43 %; the TMF stress/strain hysteresis loops' area decreases from 28.6 kJ/m^3 to 19 kJ/m^3; the peak strain decreases from 0.164 % to 0.131 %; the residual strain decreases from 0.038 % to 0.025 %; and the hysteresis modulus increases from 142 GPa to 170 GPa, as shown in Fig. 11.

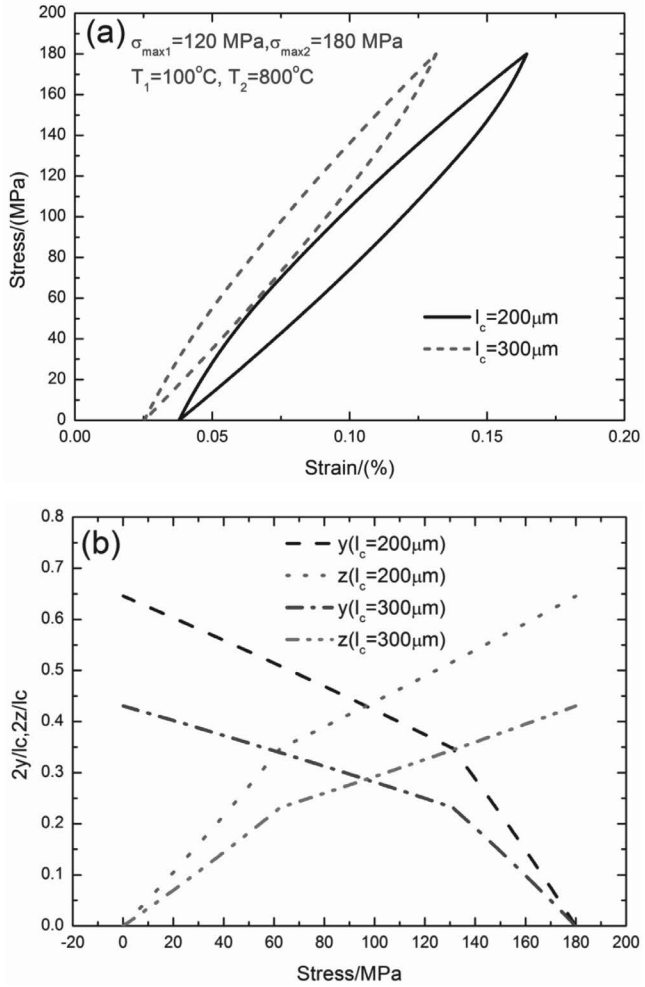

Fig. 11: The effect of matrix crack spacing (l_c = 200 and 300 μm) on (a) in-phase thermomechanical fatigue hysteresis loops; and (b) the fiber/matrix interface slip length of SiC/SiC composite under multiple loading levels of σ_{max1} = 120 MPa and σ_{max2} = 180 MPa at the temperature range of T_1 =100 °C and T_2 =800 °C.

When N = 1, 10 and 100, the TMF stress/strain hysteresis loops correspond to the partial debonding and sliding in the fiber/matrix interface debonded region; with increasing applied cycle number from N = 1 to N = 100, the fiber/matrix interface slip range increases from 41 % to 51 %; the TMF stress/strain hysteresis loops' area increases from 16.8 kJ/m^3 to 21.3 kJ/m^3; the peak strain increases from 0.128 % to 0.135 %; the residual strain increases from 0.022 % to 0.025 %; and the hysteresis modulus decreases from 170 GPa to 163 GPa, as shown in Fig. 12.

When T_1 = 100 °C, T_2 = 800 °C and T_1 = 200 °C, T_2 = 600 °C, the stress/strain TMF hysteresis loops correspond to the partial debonding and sliding in the fiber/matrix interface debonded region; with increasing thermal cyclic temperature range, the fiber/matrix interfaceslip range increases from 65 % to 67 %; the TMF stress/strain hysteresis loops' area increases from 36 kJ/m^3 to 37.3 kJ/m^3; the peak strain increases from 0.187 % to 0.192 %; the residual strain increases from 0.045 % to 0.049 %; and the hysteresis modulus decreases from 127 GPa to 125 GPa, as shown in Fig. 13.

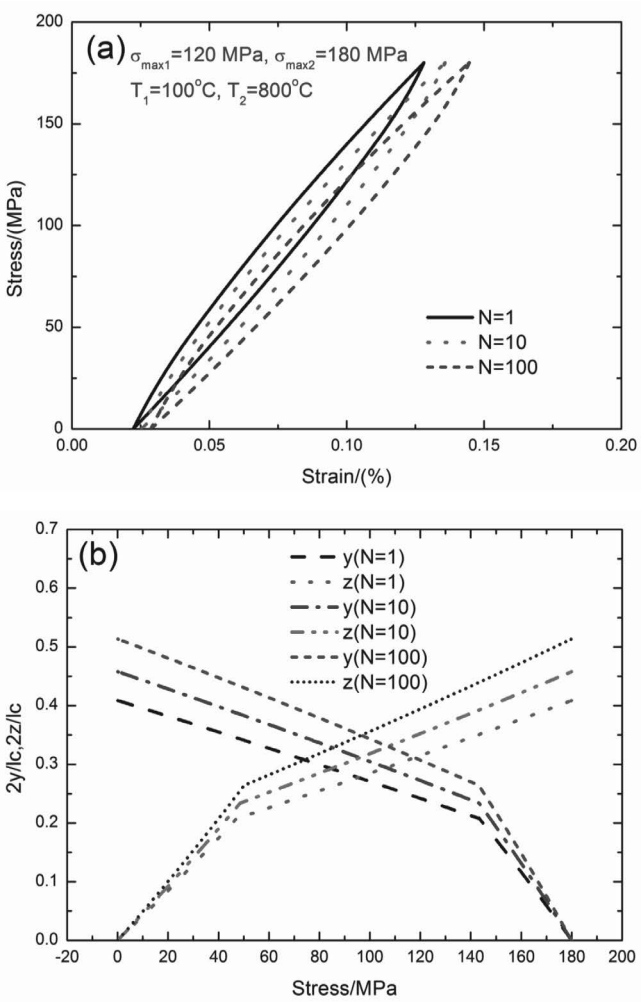

Fig. 12: The effect of the thermomechanical cycle number (N = 1, 10 and 100) on (a) in-phase thermomechanical fatigue hysteresis loops; and (b) the fiber/matrix interface slip length of SiC/SiC composite under a multiple loading sequence of σ_{max1} = 120 MPa and σ_{max2} = 180 MPa at the thermal cyclic temperature range of T_1 = 100 °C and T_2 = 800 °C.

(5) Comparisons of in-phase TMF hysteresis loops between single- and multiple-loading sequence

The comparisons of in-phase TMF stress/strain hysteresis loops and fiber/matrix interface damage state between a single-peak stress and multiple-loading sequence of σ_{max1} =120 MPa and σ_{max2} =180 MPa at the thermal cyclic temperature range of T_1 =100 °C and T_2 = 800 °C are shown in Fig. 14.

Under single-peak stress and a multiple-loading sequence, the TMF stress/strain hysteresis loops correspond to the partial debonding and sliding in the fiber/matrix interface debonded region; and the fiber/matrix interface slip lengths under the multiple-loading sequence can be divided into two regions, which are different from the fiber/matrix interface slip lengths under single-peak stress, owing to the low fiber/matrix interface shear stress in the interface wear region.

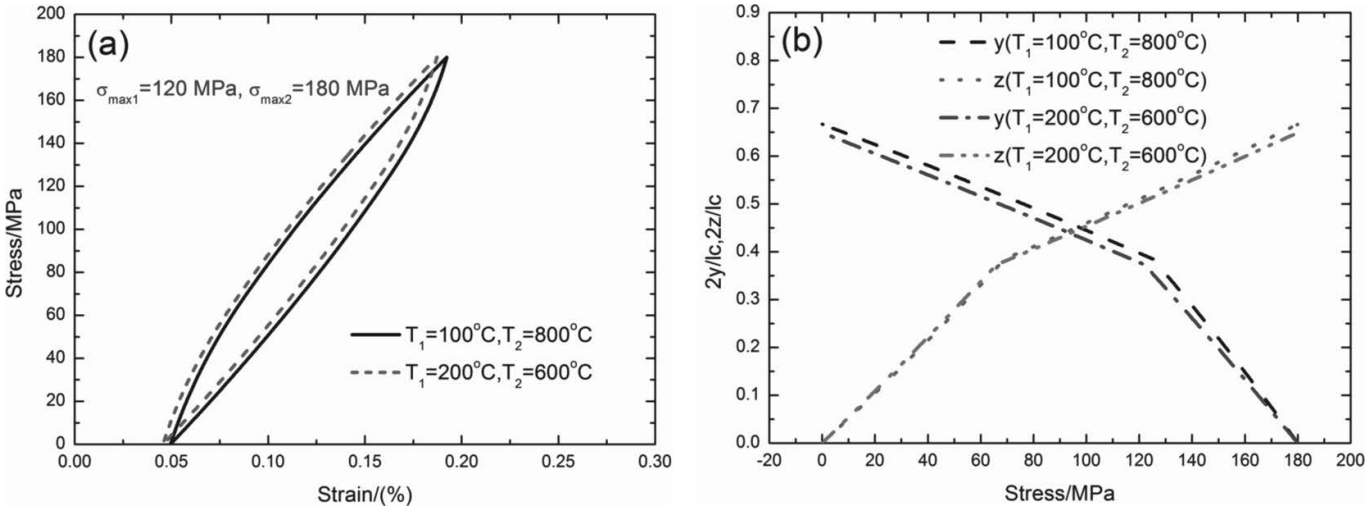

Fig. 13: The effect of temperature range (T_1 = 100 °C, T_2 = 800 °C and T_1 = 200 °C, T_2 = 600 °C) on (a) in-phase thermomechanical fatigue hysteresis loops; and (b) the fiber/matrix interface slip length of SiC/SiC composite under a multiple loading sequence of σ_{max1} =120 MPa and σ_{max2} =180 MPa at the thermal cyclic temperature range of T_1 = 100 °C and T_2 =800 °C.

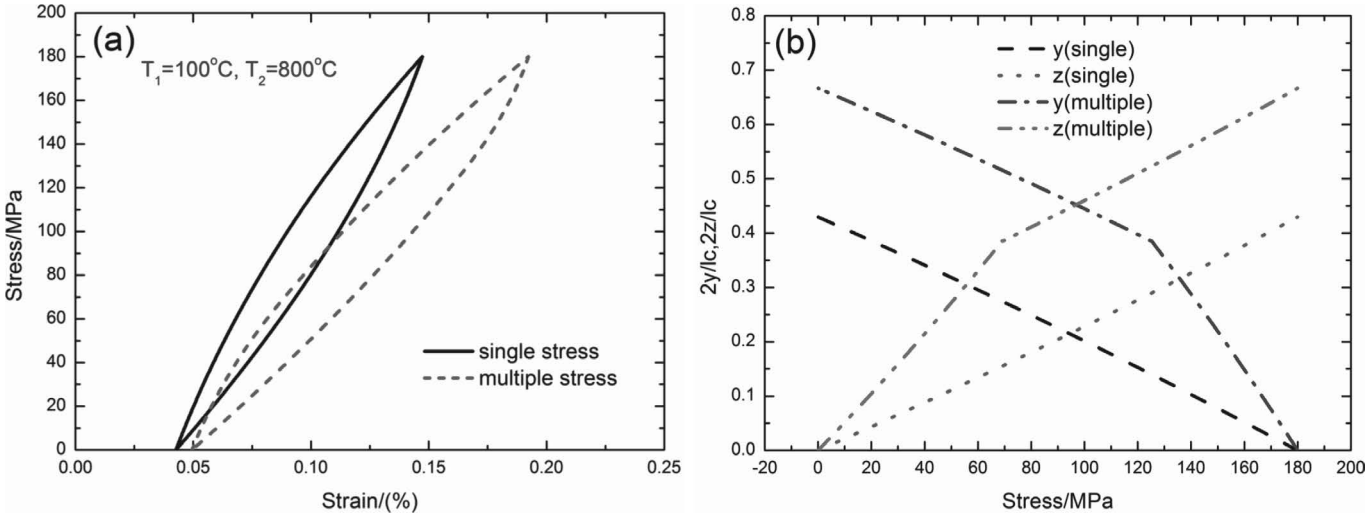

Fig. 14: (a) The fatigue hysteresis loops; and (b) the fiber/matrix interface slip lengths of SiC/SiC composite under a single- and multiple-loading sequence of σ_{max1} = 120 MPa and σ_{max2} = 180 MPa at the thermal cyclic temperature range of T_1 = 100 °C and T_2 = 800 °C.

Under multiple-loading stress levels, the fiber/matrix interface slip lengths approach 67 % of matrix crack spacing and are larger than those under single-peak stress level of 43 % of matrix crack spacing; the TMF stress/strain hysteresis loops' area increases from 26 kJ/m^3 under single-peak stress to 37.4 kJ/m^3 under multiple-loading sequence; the peak strain increases from 0.147 % to 0.192 %; the residual strain increases from 0.042 % to 0.049 %; and the hysteresis modulus decreases from 171 GPa to 126 GPa.

IV. Experimental Comparisons

Baker[35] investigated the cyclic loading/unloading stress/strain hysteresis loops of a 2D SiC/SiC composite subjected to a multiple loading sequence. The stress/strain hysteresis loops and fiber/matrix interface slip lengths of the 2D SiC/SiC composite at the multiple loading sequence of σ_{max1} =113 MPa, σ_{max2} =137 MPa and σ_{max3} = 168 MPa under cyclic loading/unloading tensile at room temperature and thermal cyclic temperature range of 100 °C and 800 °C are shown in Figs. 15 ~ 17.

The stress/strain hysteresis loops and fiber/matrix interface slip lengths of the 2D SiC/SiC composite at the first peak stress of σ_{max1} =113 MPa under cyclic loading/unloading tensile at room temperature and thermal cyclic temperature range of 100 °C and 800 °C are illustrated in Fig. 15. Under cyclic loading/unloading tensile at room temperature and in-phase TMF cyclic loading at thermal cyclic temperature range of 100 °C and 800 °C, the stress/strain hysteresis loops correspond to the partial debonding and sliding in the fiber/matrix interface debonded region, as shown in Fig. 15(a); the fiber/matrix interface slip lengths under in-phase TMF cyclic loading approach to 42.8 % of the matrix crack spacing and are larger than those under cyclic loading at room temperature of 26.6 % of matrix crack spacing; the stress/strain hysteresis loops' area increases from 9.7 kJ/m^3 under cyclic loading at room temperature to 17.8 kJ/m^3 under TMF cyclic loading; and the hysteresis modulus decreases from 88.2 GPa to 86.2 GPa, as shown in Fig. 15(b).

The stress/strain hysteresis loops and fiber/matrix interface slip lengths of the 2D SiC/SiC composite at the second peak stress of σ_{max2} =137 MPa under cyclic tensile loading/

unloading at room temperature and thermal cyclic temperature range of 100 °C and 800 °C are shown in Fig. 16. Under cyclic tensile loading/unloading at room temperature, the stress/strain hysteresis loops correspond to the complete debonding and partial sliding in the fiber/matrix interface debonded region, as shown in Fig. 16(a); under in-phase TMF cyclic loading at thermal cyclic temperature range of 100 °C and 800 °C, the stress/strain hysteresis loops correspond to the complete debonding and complete sliding in the fiber/matrix interface debonded region, as shown in Fig. 16(a); the fiber/matrix interface slip lengths under in-phase TMF cyclic loading approach 100 % of matrix crack spacing and are larger than those under cyclic loading at room temperature; the stress/strain hysteresis loops' area increases from 46.7 kJ/m^3 under cyclic loading at room temperature to 50 kJ/m^3 under TMF cyclic loading; and the hysteresis modulus decreases from 48.5 GPa under cyclic loading at room temperature to 44.4 GPa under TMF cyclic loading, as shown in Fig. 16(b).

The stress/strain hysteresis loops and fiber/matrix interface slip lengths of the 2D SiC/SiC composite at the third peak stress of σ_{max3} =168 MPa under cyclic tensile loading/unloading at room temperature and thermal cyclic temperature range of 100 °C and 800 °C are shown in Fig. 17. Under cyclic tensile loading/unloading at room temperature and in-phase TMF loading at thermal cyclic temperature range of 100 °C and 800 °C, the stress/strain hysteresis loops correspond to the complete debonding and sliding in the fiber/matrix interface debonded region, as shown in Fig. 17(a); the fiber/matrix interface slip lengths under cyclic loading at room temperature and in-phase TMF approach to 100 % of matrix crack spacing; the stress/strain hysteresis loops' area increases from 70.9 kJ/m^3 under cyclic loading at room temperature to 96.1 kJ/m^3 under TMF cyclic loading; and the hysteresis modulus decreases from 44.2 GPa under cyclic loading at room temperature to 41.5 GPa under TMF cyclic loading, as shown in Fig. 17(b).

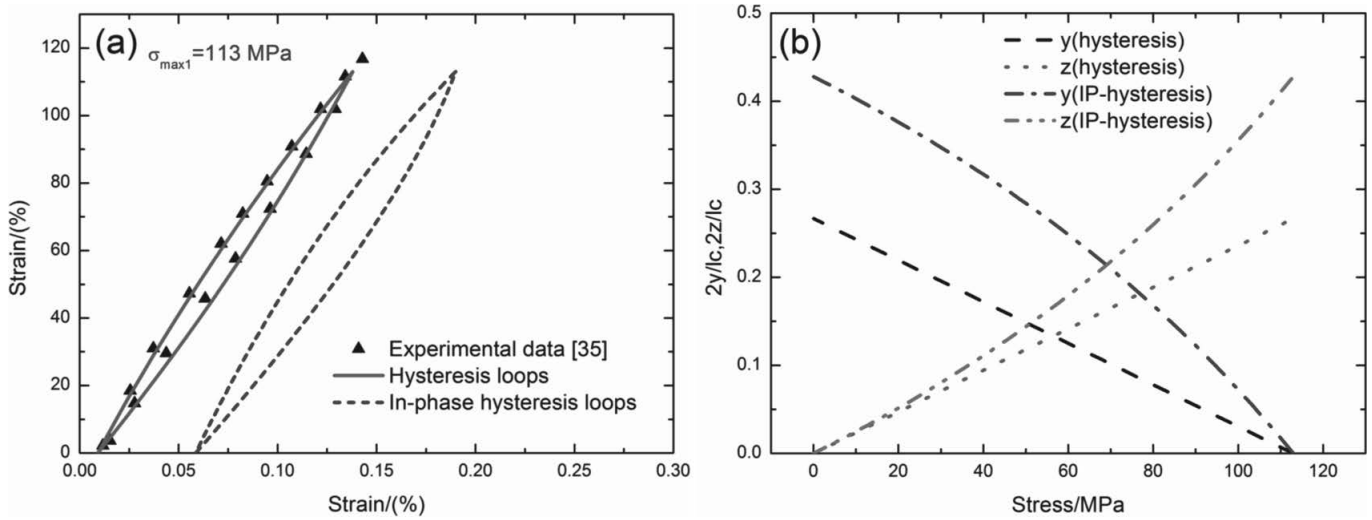

Fig. 15: (a) The fatigue hysteresis loops; and (b) the fiber/matrix interface slip lengths of the 2D SiC/SiC composite at the fatigue peak stress of σ_{max1} =113 MPa under cyclic tensile loading/unloading at room temperature and thermal cyclic temperature range of 100 °C and 800 °C.

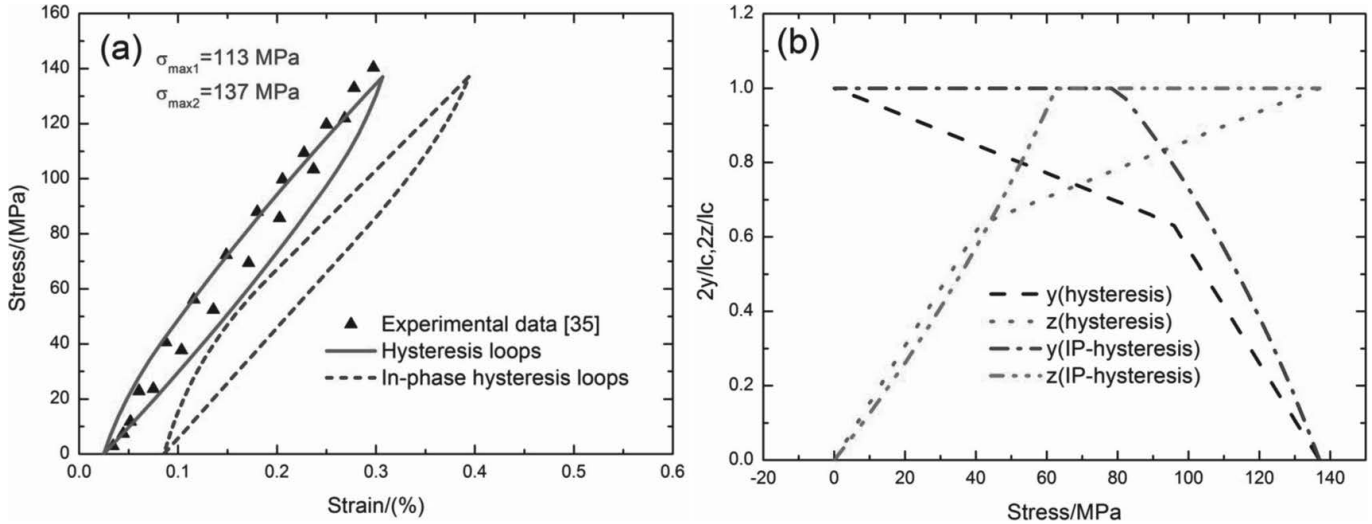

Fig. 16: (a) The fatigue hysteresis loops; and (b) the fiber/matrix interface slip lengths of the 2D SiC/SiC composite at the fatigue peak stress of σ_{max2} = 137 MPa under cyclic tensile loading/unloading at room temperature and thermal cyclic temperature range of 100 °C and 800 °C.

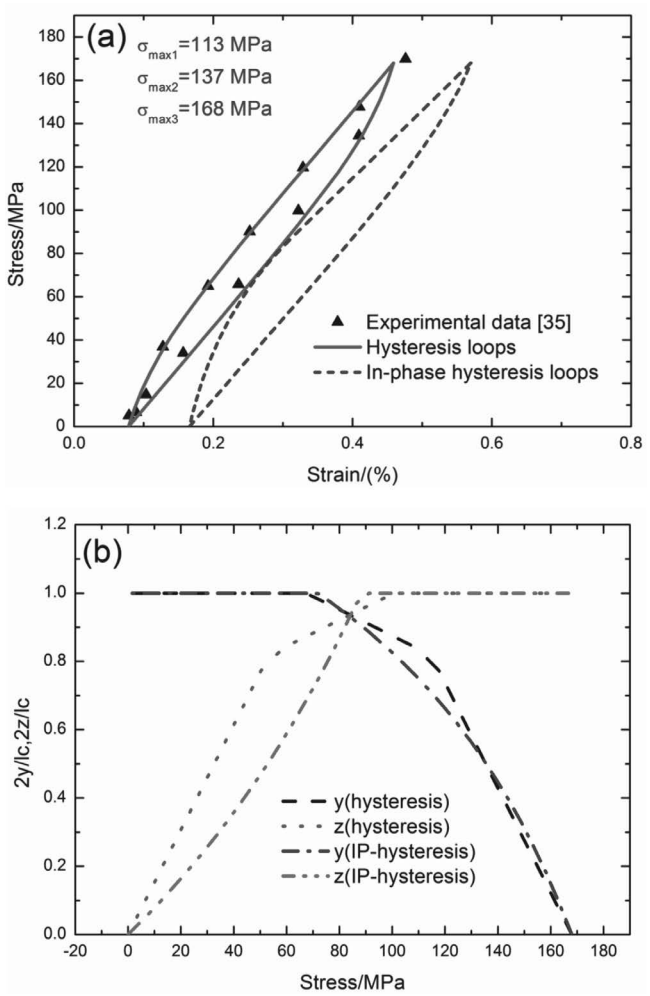

Fig. 17: (a) The fatigue hysteresis loops; and (b) the fiber/matrix interface slip lengths of the 2D SiC/SiC composite at the fatigue peak stress of σ_{max3} = 168 MPa under cyclic tensile loading/unloading at room temperature and thermal cyclic temperature range of 100 °C and 800 °C.

V. Conclusions

In this paper, the effect of a multiple-loading sequence on the in-phase TMF stress/strain hysteresis loops of SiC-CMCs has been investigated. The stress/strain hysteresis loops and fiber/matrix interface damage of a 2D SiC/SiC composite subjected to three low-high loading sequences have been predicted.

(1) Under a TMF multiple-loading sequence, the fiber/matrix interface debonding and slip lengths are larger than those under TMF single-peak stress, leading to the increase of the TMF hysteresis loops' area, peak and residual strain, and the decrease of the TMF hysteresis modulus.

(2) With increasing fiber volume fraction, fiber/matrix interface frictional shear stress, fiber/matrix interface debonded energy and fiber/matrix interface frictional coefficient, the TMF hysteresis loops' area and peak strain decrease, and the TMF hysteresis modulus increases owing to the decrease in the fiber/matrix interface slip range.

(3) With increasing matrix crack spacing, the TMF hysteresis loops' area and peak strain decrease and the TMF hysteresis modulus increases owing to the decrease of the fiber/matrix interface slip range; with increasing applied cycle numbers and thermal cyclic temperature, the TMF hysteresis loops' area and peak strain increase and the TMF hysteresis modulus decreases owing to the increase in the fiber/matrix interface slip range.

Acknowledgements

The work reported here is supported by the Fundamental Research Funds for the Central Universities (Grant no. NS2016070). The author also wishes to thank two anonymous reviewers and editors for their helpful comments on an earlier version of the paper.

References

1 Padture, N.P.: Advanced structural ceramics in aerospace propulsion, *Nat. Mater.*, **15**, 804 - 809, (2016).

2 Padture, N.P., Gell, M., Jordan, E.H.: Thermal barrier coatings for gas-turbine engine applications, *Science*, **296**, 280 - 284, (2002).

3 Li, L.B.: Damage and failure of fiber-reinforced ceramic-matrix composites subjected to cyclic fatigue, dwell-fatigue and thermomechanical fatigue, *Ceram. Int.*, **43**, 13978 - 13996, (2017).

4 Li, L.B.: Modeling strength degradation of fiber-reinforced ceramic-matrix composites under cyclic loading at room and elevated temperatures. *Mater. Sci. Eng. A*, **695**, 221 – 229, (2017).

5 Dever, J.A., Nathal, M.V., Dicarlo, J.A.: Research on high-temperature aerospace materials at NASA Glenn Research Center. *J. Aerosp. Eng.*, **26**, 500 - 514, (2013).

6 Mei, H., Cheng, L.F., Zhang, L.T.: Damage mechanisms of C/SiC composites subjected to constant load and thermal cycling in oxidizing atmosphere, *Scripta Mater.*, **54**, 163 - 168, (2006).

7 Udayakumar, A., Stalin, M., Abhayalakshmi, M.B., Hariharan, R., Balasubramanian, M.: Effect of thermal cycling of SiC/SiC composites on their mechanical properties, *J. Nucl. Mater.*, **442**, S384 - S389, (2013).

8 Dalmaz, A., Reynaud, P., Rouby, D., Fantozzi, G., Abbe, F.: Mechanical behavior and damage development during cyclic fatigue at high-temperature of a 2.5D carbon/sic composite, *Compos. Sci. Technol.*, **58**, 693 – 699, (1998).

9 Li, L.B.: Damage evolution of cross-ply ceramic-matrix composites under stress-rupture and cyclic loading at elevated temperatures in oxidizing atmosphere, *Mater. Sci. Eng. A,* **688**, 315 - 321, (2017).

10 Ruggles-Wrenn, M.B., Jones, T.P.: Tension-compression fatigue of a SiC/SiC ceramic matrix composite at elevated temperature, *J. Eng. Gas Turb. Power*, **134**, 091301, (2012).

11 Kim, T.T., Mall, S., Zawada, L.P.: Fatigue behavior of hinicalon Type-S^{TM}/BN/SiC ceramic matrix composites in a combustion environment, *Int. J. Appl. Ceram. Technol.*, **8**, 261 - 272, (2011).

12 Sabelkin, V., Zawada, L.P., Mall, S.: Effects of combustion and salt-fog exposure on fatigue behavior of two ceramic matrix composites and a superalloy, *J. Mater. Sci.*, **50**, 5204 - 5213, (2015).

13 Li, L.B.: Modeling thermomechanical fatigue hysteresis loops of long-fiber-reinforced ceramic-matrix composites under out-of-phase cyclic loading condition, *Int. J. Fatigue*, **105**, 34 - 42, (2017).

14 Holmes, J.W., Cho, C.D.: Experimental observations of frictional heating in fiber-reinforced ceramics, *J. Am. Ceram. Soc.*, **75**, 929 - 938, (1992).

15 Rouby, D., Reynaud, P.: Fatigue behavior related to interface modification during load cycling in ceramic-matrix fiber composites, *Compos. Sci. Technol.*, **48**, 109 - 118, (1993).

16 Evans, A.G., Zok, F.W., McMeeking, R.M.: Fatigue of ceramic matrix composites, *Acta Metall. Mater.*, **43**, 859 - 875, (1995).

[17] Mizuno, M., Zhu, S.J., Kagawa, Y., Kaya, H.: Stress, strain and elastic modulus behavior of SiC/SiC composites during creep and cyclic fatigue, *J. Eur. Ceram. Soc.*, **18**, 1869 - 1878, (1998).

[18] Lee, S.S., Zawada, L.P., Staehler, J.M., Folsom, C.A.: Mechanical behavior and high-temperature performance of a woven Nicalon™/Si-N-C ceramic-matrix composite, *J. Am. Ceram. Soc.*, **81**, 1797 - 1811, (1998).

[19] Fantozzi, G., Reynaud, P., Rouby, D.: Thermomechanical behavior of long fibers ceramic-ceramic composites, *Sil. Ind.*, **66**, 109 - 119, (2001).

[20] Staehler, J.M., Mall, S., Zawada, L.P.: Frequency dependence of high-cycle fatigue behavior of CVI C/SiC at room temperature, *Compos. Sci. Technol.*, **63**, 2121 - 2131, (2003).

[21] Roth, D.J., Verrilli, M.J., Martin, R.E., Cosgriff, L.M.: Initial attempt to characterize oxidation damage in C/SiC composite using an ultrasonic guide wave method, *J. Am. Ceram. Soc.*, **88**, 2164 - 2168, (2005).

[22] Mall, S., Engesser, J.M.: Effects of frequency on fatigue behavior of CVI C/SiC at elevated temperature, *Compos. Sci. Technol.*, **66**, 863 - 874, (2006).

[23] Halbig, M.C., McGuffin-Cawley, J.D., Eckel A.J., Brewer, D.N.: Oxidation kinetics and stress effects for the oxidation of continuous carbon fibers within a microcracked C/SiC ceramic matrix composite, *J. Am. Ceram. Soc.*, **91**, 519 - 526, (2008).

[24] Zhang, C.Y., Wang, X.W., Liu, Y.S., Wang, B., Han, D., Qiao, S.R., Guo, Y.: Tensile fatigue of a 2.5D-C/SiC composite at room temperature and 900 °C, *Mater. Design*, **49**, 814 - 819, (2013).

[25] Zhang, Y.N., Cheng, L.F., Zhang, L.T., Luan, X.G.: Comparative analysis of low-cycle fatigue behavior of 2D-C_f-PyC/SiC composites in different environments, *Int. J. Appl. Ceram. Technol.*, **12**, 491 - 499, (2015).

[26] Luo, Z., Cao, H., Ren, H., Zhou, X.G.: Tension-tension fatigue behavior of a PIP SiC/SiC composite at elevated temperature in air, *Ceram. Int.*, **42**, 3250 - 3260, (2016).

[27] Li, Y., Xiao, P., Li, Z., Zhou, W., Liensdorf, T., Freudenberg, W., Langhof, N., Krenkel, W.: Tensile fatigue behavior of plain-weave reinforced C_f/C-SiC composites. *Ceram.Int.*, **42**, 6850 - 6857, (2016).

[28] Dong, N., Zuo, X.Z., Liu, Y.S., Zhang, L.T., Cheng, L.F.: Fatigue behavior of 2D C/SiC composites modified with Si-B-C ceramic in static air, *J. Eur. Ceram. Soc.*, **36**, 3691 - 3696, (2016).

[29] Reynaud, P., Douby, D., Fantozzi, G.: Effects of temperature and of oxidation on the interfacial shear stress between fibers and matrix in ceramic-matrix composites, *Acta Mater.*, **46**, 2461 – 2469, (1998).

[30] Li, L.B.: Modeling for cyclic loading/unloading hysteresis loops of carbon fiber-reinforced ceramic-matrix composites at room and elevated temperatures. Part I: Theoretical analysis, *Eng. Fract. Mech.*, **164**, 117 – 136, (2016).

[31] Li, L.B.: Modeling for cyclic loading/unloading hysteresis loops of carbon fiber-reinforced ceramic-matrix composites at room and elevated temperatures. Part II: Experimental comparisons, *Eng. Fract. Mech.*, **164**, 137 – 154, (2016).

[32] Evans, A.G.: Design and life prediction issues for high-temperature engineering ceramics and their composites, *Acta Mater.*, **45**, 23 – 40, (1997).

[33] Gao, Y., Mai, Y., Cotterell, B.: Fracture of fiber-reinforced materials, *J. Appl. Math. Phys., 39, 550 – 572*, (1988).

[34] Budiansky, B., Hutchinson, J.W., Evans, A.G.: Matrix fracture in fiber-reinforced ceramics, *J. Mech. Phys. Solids*, **34**, 167 - 189, (1986).

[35] Baker, C.R.: Assessing damage in composite materials, PhD thesis, University of Akron, Ohio, USA, 2014.